J Mater Sci (2008) 43:942–951
DOI 10.1007/s10853-007-2208-3

Nd:YAG laser surface melting of aluminium alloy 6013 for improving pitting corrosion fatigue resistance

W. L. Xu · T. M. Yue · H. C. Man

Received: 17 July 2007 / Accepted: 4 October 2007 / Published online: 9 November 2007

Abstract Laser surface treatment of aluminium alloy 6013 was conducted with the aim of improving the alloy's resistance to pitting corrosion fatigue. The study showed that laser melting using a high power Nd:YAG laser increased the resistance of the alloy to pitting corrosion and pitting corrosion fatigue. As corrosion pits are favourable sites for the initiation of fatigue cracks, and the process of crack initiation often takes up most of the fatigue life, especially at low stress levels, a high pitting corrosion resistance resulted from the laser treatment improved fatigue crack initiation resistance. With regard to fatigue crack propagation, although interdendritic boundaries are vulnerable to corrosion attacks due to the presence of second phase particles, nonetheless, due to the nature of the rough and undulating fracture surface, fatigue growth would be retarded. Under the present experimental conditions, the improvement in corrosion resistance brought about by laser surface melting was found to prevail over the adverse effect caused by the residual stresses induced by laser melting.

Introduction

High-strength aluminium alloys (HSAL) are widely used in aircraft and other heavy stress-bearing engineering structures due to their high specific mechanical properties. However, these alloys are susceptible to stress-related corrosion, such as stress corrosion cracking and corrosion fatigue, particularly in the presence of chloride-containing media [1, 2]. Thus, in service, the combined effect of corrosion and loading on a high strength aluminium alloy structure can dramatically decrease its service life. The degradation of these materials caused by the interactions of corrosion and mechanical stress is a matter of major concern, particularly because many structural parts are inaccessible for inspection and cannot be monitored. In the case of corrosion fatigue, the corrosion defect(s) may reach a critical length for fatigue cracks to develop and result in catastrophic failures. In fact, fatigue life can be markedly reduced by accelerated crack initiation from corrosion features such as pits that act as stress raisers. Since corrosion fatigue is a conjoint effect of an active environment and cyclic loading, it is inevitably influenced by the nature of the loading as well as the type of corrosion. Indeed, many previous studies have shown that pitting corrosion can cause a dramatic reduction in the fatigue life of HSAL [3, 4].

During the past few decades, owing to the combined efforts of material scientists and engineers, the problems of stress-related corrosion have largely been contained. Advances made in surface treatments and coatings have overcome some forms of stress-related corrosion. Currently, the corrosion of HSAL is mainly prevented by the application of corrosion protective systems, including inhibitors, anodising, conversion coatings, primers, and paint finishes. However, these remedial methods are not without penalties and have their own limitations. For instance, the presence of defects in the anodized coating [5] and the low yield strength of the clad layer are possible reasons for causing a lowering of fatigue resistance. Thus, it is clear that, not withstanding the excellent achievements that scientists and engineers have had in

W. L. Xu · T. M. Yue (✉) · H. C. Man
The Advanced Manufacturing Technology Research Centre, Department of Industrial and Systems Engineering, The Hong Kong Polytechnic University, Hung Hom, Hong Kong
e-mail: mftmyue@inet.polyu.edu.hk

combating the problems of stress-related corrosion in HSAL, it is necessary to search continuously for further solutions.

In the search for alternative methods to combat the various corrosion problems of HSAL, laser surface melting (LSM), has attracted growing interest in recent years. However, much attention has been given to the study of the effect of LSM on the electrochemical behaviour of aluminium alloys when tested under the no external loads condition [6–8]. With regard to the problems of stress-related corrosion, our knowledge on the ability of LSM for improving the resistance to pitting corrosion fatigue is still limited. The problem of corrosion fatigue in HSAL has received considerable attention during the past 50 years. Although, the fundamental problem of corrosion fatigue is thought to be the continuous destruction of dislocation barriers and solute atoms within the crystals themselves (anodic slip-band cracking), however, for HSAL, the particular problem of pitting corrosion fatigue is one of the main topics of concern. This is due to the high susceptibility of HSAL to pitting corrosion. Pao [9] found that the presence of pre-existing corrosion pits in the 7075 aluminium alloy, shortened the fatigue crack initiation life of the alloy by a factor of two to three and decreased the fatigue crack initiation threshold by about 50%. Recognizing this problem, the present research study aims to employ LSM to tackle a specific corrosion initiated fatigue problem, namely, pitting corrosion fatigue in HSAL.

Experimental

Material

Aluminium alloy 6013, a material widely used in the fuselages of aircraft is used for this investigation. Al-alloy 6013 is a high-strength aluminium alloy developed by Alcoa to replace the traditional alloy 2024-T3 [10]. When compared to 2024-T3, 6013-T6 has 12% higher tensile strength, 30% higher compression yield strength, 3% lower density, and a similar level of fracture toughness. Moreover, it is claimed that the alloy is virtually immune to exfoliation cracking. However, this alloy is susceptible to pitting and intergranular corrosion [11, 12]. The material used in this investigation was supplied by Alcoa in the form of 40 mm thick plates, which were produced by rolling to a cold finished surface. The chemical composition of 6013-T651 is given in Table 1. The T651 condition involved heat treatment at a solution temperature of 475 °C for 1 h, then quenching with water to room temperature, followed by a 2% stretch, and an aging treatment of 24 h at 120 °C.

Laser surface melting

Laser surface melting was undertaken using a continuous wave (CW) high-power Nd:YAG laser system (Lumonics MW 2000). One of the advantages of using a Nd:YAG laser instead of a CO_2 laser is that aluminium alloys have a higher absorption coefficient at a radiation wavelength of 1.06 μm (Nd:YAG) compared to 10.6 μm (CO_2). The laser beam was transmitted by means of an optical fibre and focused onto the specimen by a BK-7 glass lens with a focal length of 80 mm. Pure nitrogen was used as shielding gas with a flow rate of 25 L/min passing through a glove box. After a number of trials, the processing parameters were chosen: power energy of 700 W, scanning velocity of 25 mm/min, defocusing distance of 3 mm, and 50% track overlapping. These conditions were selected as they can produce a relatively smooth and crack free re-solidified surface. In the treating of the fatigue specimen, the laser tracks are running parallel to longitudinal axis of the specimen. Prior to laser treatment, all the specimens were sand-blasted using Al_2O_3 particles for increasing the absorption of laser irradiation.

Microstructure characterization

The surface morphology, chemical composition, phases, and the characteristics of the laser-treated specimens were analysed by scanning electron microscopy (SEM), energy dispersive X-ray spectroscopy (EDX), X-ray diffraction (XRD) and transmission electron microscopy (TEM). The microstructure of the laser-treated zone was studied in detail by cross-sectional TEM. To prepare for the TEM examination, two specimens were glued together using epoxy resin, with the two laser-treated surfaces facing each other. The glued pieces were mechanically ground and polished along the cross-sectional plane to a thickness of about 10 μm. This was followed by ion milling, which was performed by Ar^+ bombardment at 5 keV. Initially, the angle of ion milling was set at 10°; at the final stage, an angle of 7° was used and processing was performed at 3 keV to guarantee a large enough thin area.

Residual stress measurement

The residual stress at the surface of the corrosion fatigue specimen was measured in order to identify whether residual stresses might have a significant effect on the corrosion fatigue properties. In fact, any substantial residual tensile stresses present at the surface of the specimen might lower the fatigue strength. The residual stress induced by laser treatment was measured by the $\mathrm{Sin}^2\psi$

Table 1 Chemical composition of aluminium alloy 6013

	Si	Fe	Cu	Mn	Mg	Cr	Zn	Ti	Other	Al
wt%	0.6–1.0	0.5	0.6–1.1	0.2–0.8	0.8–1.2	0.1	0.25	0.1	0.15	Balance

method, making use of the diffraction peak of (311) at $2\theta = 78.227°$ of aluminium. Crystalline planes at higher diffraction angles were not chosen due to the equipment limit on the scanning range. XRD spectra were collected by an X-ray diffractometer, scanning from 74° to 82°, using a step size of 0.02°.

Electrochemical tests

The potentiodynamic polarization test is a fairly simple and highly effective method for determining corrosion performance, such as pitting potential and corrosion current density, of aluminium alloys. However, the measured current response primarily reflects the corrosion activities of the vulnerable corrosion sites on the surface of the specimen and does not provide enough information of the resistance of the surface film/coating as a whole. Given this constraint, it is considered that electrochemical impedance spectroscopy (EIS), which is capable of characterizing the properties of a wide range of films and coatings against corrosion, should also be used to supplement the deficiency of the polarization test. The potentiodynamic test was conducted in a 3.5% neutral aerated NaCl solution. In the experiment, a classical electrochemical cell consisting of three electrodes was used: a working electrode, two counter electrodes made of graphite and a reference electrode (a saturated calomel electrode (SCE)). The exposed area of the working electrode was 1 cm^2; and an initial delay time of 3,600 s was employed for the specimen to reach a stable condition. The polarization scan commenced at −110 mV below the steady open-circuit potential (OCP) at a scanning rate of 0.2 mV/s. For the EIS measurements, a sinusoidal voltage of 5 mV and a frequency range of 3×10^5–10^{-2} Hz were used.

Corrosion fatigue test

The corrosion fatigue test was conducted under the pull-pull loading condition using a direct stress fatigue machine. The fatigue specimens were extracted from the plate along the rolling direction, and were in the form of a cylindrical dog-bone with a minimum diameter of 3.4 mm. The specimens were tested in a corrosion cell comprising a graphite counter electrode and a saturated calomel reference electrode. The current/time response of the specimen was recorded during fatigue testing. This information is very valuable for assessing the integrity of the surface film, which is closely related to the corrosion damage of the surface. The fatigue specimen was prepared under the guidelines of ASTM E466. The fatigue test was conducted with a stress ratio $R = 0.5$ at a maximum stress of 65 MPa, and at a frequency of 400 cycle/min. The idea of using such a relatively low testing frequency is to provide a favourable environment to allow the effect of pitting corrosion on fatigue strength to be revealed.

Results and discussion

Microstructure and residual stress

Figure 1 shows the microstructure of a cross section of a laser-treated specimen, in which a crack-free melt layer of thickness in the order of 500 μm formed at the surface. The layer consists of a fine dendritic structure, which unlike the untreated material, has no coarse constituent particles and only fine interdendritic phases were present (Fig. 2). Compared to the constituent particles in the untreated zone, which commonly have sizes of over 10 μm (Fig. 3), the interdendritic phases in the laser-melted layer were much smaller, normally less than 1 μm. This is caused by the extremely fast solidification rate resulting from the quenching action of the substrate. Regarding the untreated wrought alloy, since it was formed by continuous casting in thick sections, coarse intermetallics were expected and they could not be readily taken into solution even after heat treatment.

The solidification of the molten pool began with epitaxial growth at the fusion boundary (Fig. 1a). This also happened in boundaries between two passes of laser melting (Fig. 1b). It is apparent that columnar crystal growth had dominated the initial solidification process, and equiaxed crystal growth was experienced towards the centre of the melt pool. This is considered to be related to the melt pool's thermal gradient in relation to the condition of columnar-to-equiaxed transition (CET). In laser melting, the temperature gradient is highest when solidification is first initiated, then decreases as solidification approaches the melt pool's surface. Such conditions would facilitate CET towards the surface of the molten pool [13]. It is considered that if the entire re-melt layer comprises columnar crystals, it would be detrimental to the corrosion resistance of the material, since corrosion attacks could follow the rather straight path of the boundary of columnar grains. The compositions of some interdendritic phases

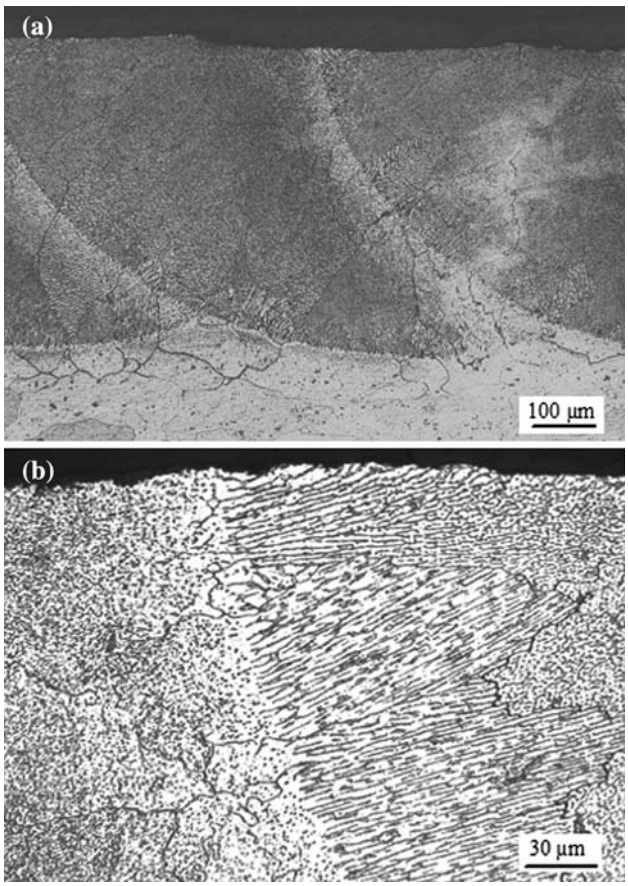

Fig. 1 Microstructure of a laser-treated specimen: (**a**) overall view; (**b**) enlarged view of the fusion boundary between two laser passes, showing epitaxial growth of crystals

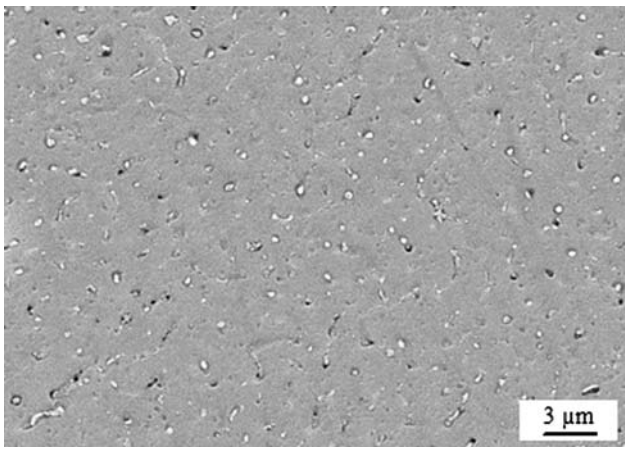

Fig. 2 Backscattered electron image of the fusion zone, showing fine interdendritic phases

were analysed by EDX, and the results revealed that they are primarily enriched in Cu, Mn, and Fe. The enrichment of alloying elements was considered to be the result of non-equilibrium solidification, with high solidification rates. It has been reported that Al–Cu–Mn–Fe phases are cathodic

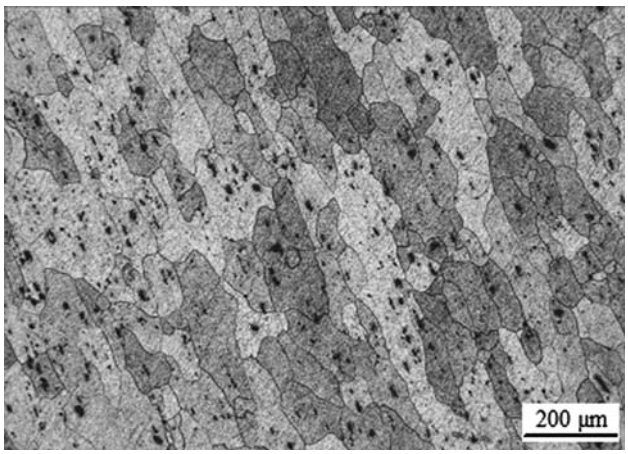

Fig. 3 Microstructure of untreated aluminium alloy 6013-T651 showing the presence of coarse constituent particles in the matrix

as compared to the surrounding aluminium matrix [14]. The galvanic coupling between interdendritic phases and the matrix material could cause the dissolution of the anodic phase.

The TEM analysis indicated that after Nd:YAG laser treatment, a film about 1 μm thick formed at the surface of the specimens (Fig. 4). Since the results of the XRD analysis detected an AlN phase at the surface of laser-melted zone (Fig. 5), it is believed that this film primarily consists of AlN, which has a grain size of the order of 50 nm (Fig. 6). This is much larger than that formed in excimer laser treatment [15], where the grain size of the surface film is of the order of 10 nm. The reason for the difference in grain size is believed to be caused by a much higher cooling rate experienced in the case of excimer melting. The formation of this film was the result of the reaction of the laser-excited active nitrogen ions with the solidified surface. It is envisaged that the AlN phase formed by Nd:YAG laser treatment would enhance the corrosion resistance of the alloy. The AlN phase that formed in the surface, which is normally considered an electrical insulator, behaves as a barrier to prevent the flow of electrons, and would thus reduce the rate of chemical reaction.

On the basis of the XRD results, the residual stress at the surface of the laser-treated specimen was determined (Table 2). It is apparent that tensile residual stresses were created at the surface of the specimen. The residual stresses produced were much lower than those measured on single laser-melted tracks of aluminium alloy 2014 [16]. This is probably attributed to the post-heating effect as a result of a large percentage of track overlapping.

Pitting corrosion behaviour

The typical polarization curves of the untreated and the laser-treated specimens tested in 3.5% NaCl solution are

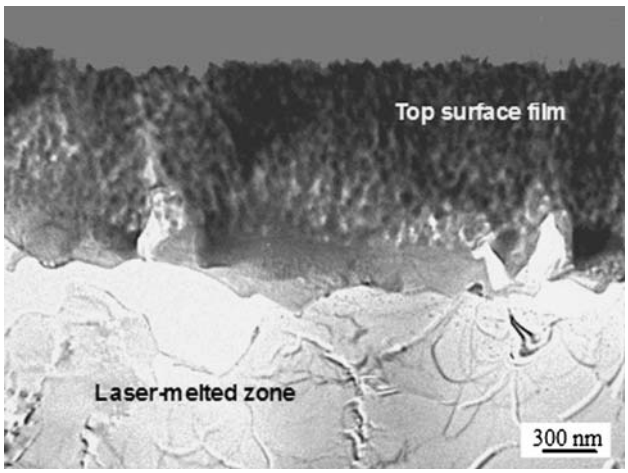

Fig. 4 TEM micrograph showing a film structure formed at the surface of the laser-treated specimen

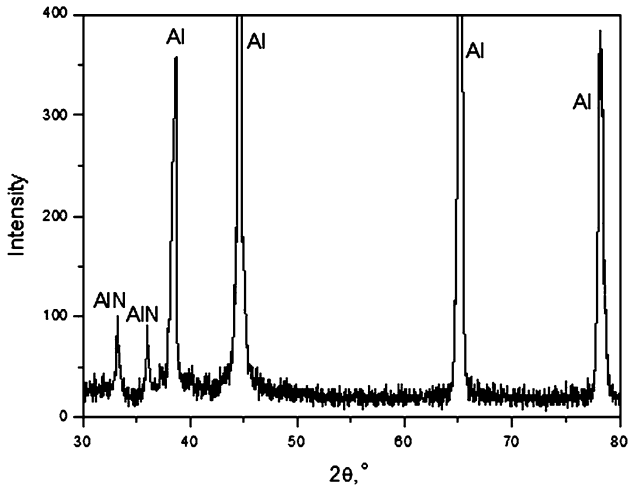

Fig. 5 XRD spectrum of the laser-treated specimen

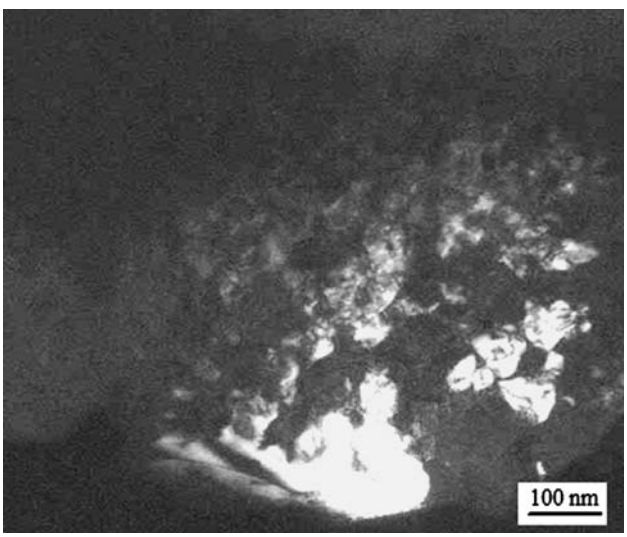

Fig. 6 Dark field image of the grain structure of the surface film

presented in Fig. 7. Similar to most aluminium alloys, the untreated 6013 alloy exhibited an active anodic dissolution in the entire range of the anodic potentials, i.e. the pitting potential was virtually the same as the corrosion potential. This strongly indicates the low pitting resistance of the alloy in the 3.5% NaCl solution. In contrast, the corrosion potential of the laser-treated specimen shifted to a more positive direction (from −710 mV to −690 mV), and the pitting potential was also uplifted to −643 mV. In addition, a low corrosion current density was obtained, which was one order lower in magnitude than that of the untreated specimen.

The results of the potentiodynamic polarization test showed that the pitting resistance of the alloy was improved by LSM. Blanc [17] and Guillaumin [18] reported that coarse intermetallic particles present in the 6056 alloy (the French equivalent to the 6013 alloy) were the major sources for the nucleation of pits, subsequently leading to intergranular cracking. Thus, the improvement in pitting resistance of 6013 could be attributed to the elimination of the coarse particles in the as-received material, as well as the forming of the AlN surface film. The AlN phase, which acts as an insulator provides a barrier to inhibit electrochemical attack to the re-melt layer underneath. However, an examination of the laser-treated specimen which had been subjected to the potentiodynamic polarization test (Fig. 8) showed that preferential dissolution of the dendrite cores generally occurred in the YAG laser-treated specimen, in which most of the second phase particles behaved as cathodic sites and the dendrite cells as anodic sites. So it appears that although the AlN film produced at the surface of the laser-treated specimen would no doubt increase the initial corrosion resistance of the material, it is also evident that the microstructure of the re-melt layer underneath plays an important role in governing the overall corrosion behaviour of the laser-treated material. This is of particular importance after prolonged corrosion attack where the surface film of AlN had been corroded away.

The results of the TEM analysis showed that a 500 μm thick re-melted layer with a thin surface nitride film formed after the laser treatment. To understand the degradation behaviour of the surface film and the re-melted layer, EIS measurements were taken at different immersion times of 0.5, 2, and 6 h. Figure 9 depicts the time dependence of the EIS results, which shows that the impedance spectra for both the untreated and the laser-treated specimens comprises of two semicircles. As the immersion time increased, the radii of the semicircles gradually decreased, indicating a decrease in impedance. By comparing the radii of the semicircles, the laser-treated specimens were found to possess much higher impedance, up to five times higher than that of the untreated specimens. Even after 6 hours of

Table 2 Residual stress measured for the laser-treated specimen

	Measurement 1	Measurement 2	Measurement 3	Average
Residual stress (MPa)	85 ± 11	104 ± 25	107 ± 17	99 ± 18

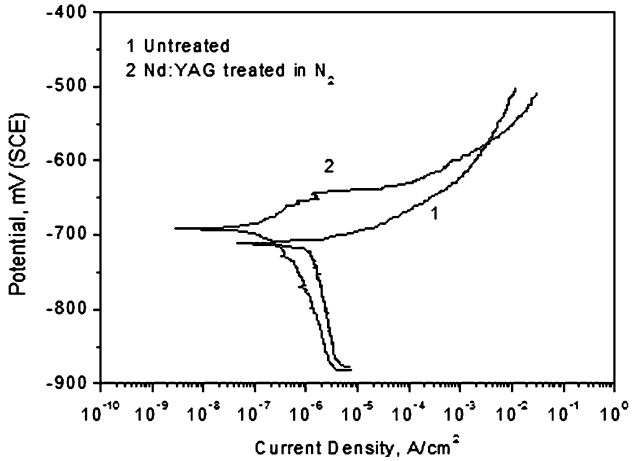

Fig. 7 Potentiodynamic polarization curves of the untreated laser-treated specimens

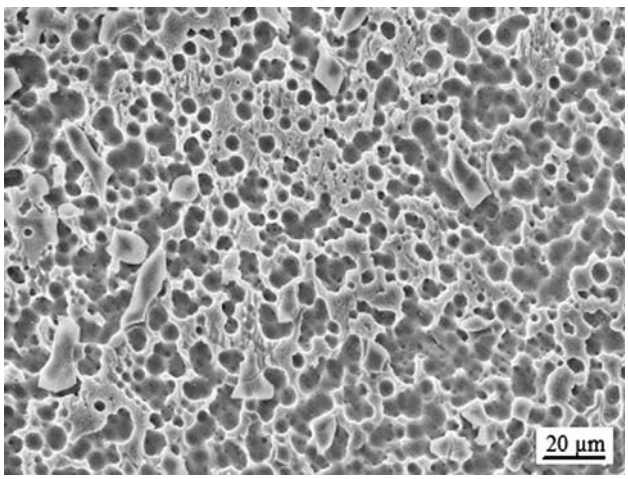

Fig. 8 Corroded surface of a laser-treated specimen after the potentiodynamic polarization test

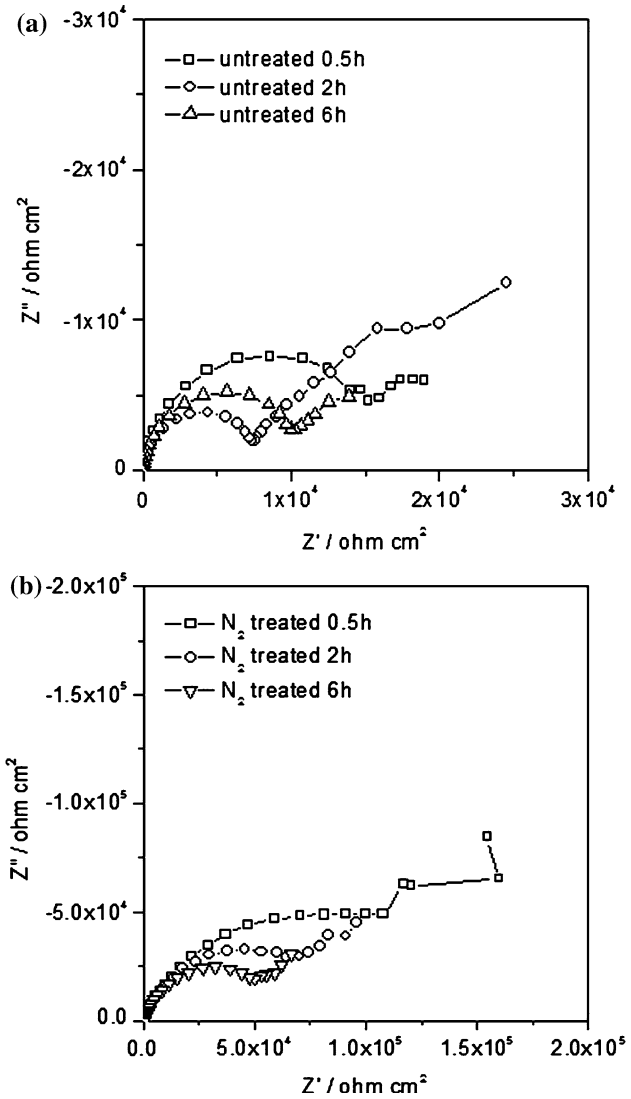

Fig. 9 Nyquist plots of (**a**) the untreated specimen; (**b**) laser-treated specimen

immersion, the radius of the first semicircle of the laser-treated specimen was still higher than that of the untreated specimen.

According to the microstructure of the laser-treated specimens, where the laser-treated layer can be broadly divided into two layers, i.e. the surface AlN film and the re-solidified dendritic layer, a two-constant equivalent circuit (Fig. 10) was proposed to simulate the electrochemical corrosion reactions at the surface of the specimen. This is coherent with the results of the impedance measurements, where two semicircles occurred within the measuring frequencies. It is assumed that each semicircle corresponds to one kind of electrochemical reaction; the one that appeared at high frequencies was associated with the reaction of the film, while the one that appeared at low frequencies was related to the reaction of the re-melted layer. In the present study, a constant phase element (CPE) instead of a pure capacitor was used to represent the non-ideal capacitive behaviour of the corrosion system, because the surface under investigation was not entirely homogeneous, and the lack of homogeneity and the consequently induced dispersion effects were better modelled with a CPE [19]. The impedance of the CPE is given by $Z_{\mathrm{CPE}} = Y_0^{-1}(\mathrm{j}\omega)^{-n}$,

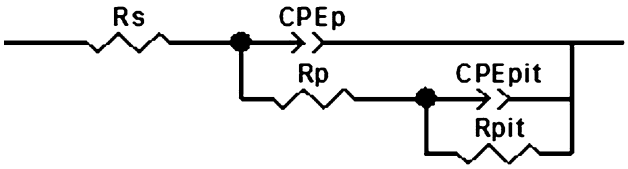

Fig. 10 Equivalent circuit model for the untreated and laser-treated specimens: R_s, resistance of the solution; R_p, polarization resistance of the passive surface; CPE_p, capacitance of the passive surface; R_{pit}, polarization resistance associated with localized dissolution; CPE_{pit}, capacitance associated with localized dissolution

where Y_0 is the magnitude of the CPE and n is the exponential term. For pure capacitors, n is equal to 1; while for a corrosion system, depending on the roughness and the integrity of the surface film, n has a value between 0 and 1.

Table 3 shows the fitted results of the EIS plots of the laser-treated specimens. The decrease in R_p and R_{pit} suggested that there was a decrease in film resistance and pitting resistance with time. Apparently, the YAG laser-formed surface film had higher R_p and R_{pit} values than those of the untreated specimens. However, when compared to excimer laser treatment [15], the improvement gained over the untreated material by YAG laser treatment was significantly less, despite a thicker film being produced by YAG laser treatment, and this is true for both the values of R_p and R_{pit}. This indicates that both the surface AlN film and the re-melted layer produced by the YAG laser treatment have less resistance to corrosion than those formed by the excimer laser treatment. With regard to the different film resistance, the reason for this is still unclear. However, the much refined grain structure of the AlN phase formed in the excimer laser-treated material could be a significant factor causing its superior film resistance. Regarding the resistance of the re-melt layer, previous studies have reported that second phase particles and precipitates in aluminium alloys can exert a negative effect on the continuity of the oxide film, and thus cause poor corrosion resistance [20]. In the case of YAG laser treatment, the dendritic structures present in the re-melted layer are vulnerable to corrosion attack.

Pitting corrosion fatigue behaviour

Figure 11 summarises the corrosion fatigue life of the untreated and laser-treated specimens. The results reveal that the fatigue life of 6013 alloy was prolonged after the laser treatment. The corresponding corrosion currents recorded for these specimens are given in Fig. 12. The current density of the laser-treated specimen was found to be extremely low, with a value below 10^{-5} A/cm^2 up to the number of fatigue cycles of 10^5. As a whole, the current density of the laser-treated specimen is at least one order lower in magnitude than that of the untreated specimen for most of the test period.

The longitudinal surface of the laser-treated specimen after corrosion fatigue testing was examined (Fig. 13a), and was found to be different from the untreated specimen (Fig. 13b). No severe active dissolution was observed at the surface of the laser-treated specimen, except for some dispersed corrosion pits. An examination of the fracture surface of the laser-treated specimen showed that the main fracture surface was joined by several terrace steps. This gives rise to an undulating appearance (Fig. 14a), with little evidence of heavy corrosion attack on the interior of the specimen. This is different from the heavily corroded fracture surface of the untreated specimen (Fig. 14b). The badly corroded area is believed to be a result of relatively little time being spent on crack initiation and most of the fatigue life was spent on crack propagation. As such, the fatigued area had been subject to prolonged corrosion attack, and corrosion has destroyed the fatigue features on the fracture surface. This makes it impossible to tell whether intergranular cracking was in any way involved in the initiation and growth of fatigue cracks and it was difficult to identify the fatigue origin(s). These observations thus show that laser treatment increased the fatigue initiation resistance of the alloy.

The improvement in corrosion fatigue resistance is believed to be due to the initiation of fatigue cracks at corrosion pits, which can be effectively retarded by laser treatment as a result of the formation of a compact nitride film at the surface, in which the surface film separates the aggressive solution from the base metal. With regard to crack propagation behaviour within the re-melt layer, a rough fracture surface was obtained. This is considered to be related to the dendritic structure formed in the re-melted zone. In this case, the fatigue crack primarily followed the interdendritic boundaries. This has been confirmed by examining a section of a fatigued specimen, in which secondary fatigue cracks were found to follow the interdendritic boundaries (Fig. 15). This is different from most wrought aluminium alloys, in which, corrosion fatigue cracks grow in a transgranular manner. Apparently, in the case of Nd:YAG laser treatment, the interdendritic boundaries are vulnerable to corrosion attack due to the presence of second phase particles. Nonetheless, on the basis of the rough and undulating fracture surface of the laser-treated specimens, it could be anticipated that fatigue growth would be retarded. This is because a tortuous, interdendritic crack path with crack branching will reduce the effective stress intensity at crack tips [21], leading to roughness-induced crack closure [22]. In addition, the hindering effect at the crack tip coming from the interdendritic particles has also been reported to be beneficial for a high fatigue cracking resistance [23].

Table 3 A summary of the fitted results of the components of the equivalent circuit

Specimen	CPE_p		R_p (Ω cm^2)	CPE_{pit}		R_{pit} (Ω cm^2)
	Y_0 (Fcm^{-2} Hz^{1-n})	n		Y_0 (Fcm^{-2} Hz^{1-n})	n	
Untreated						
0.5 h	6.29E-6	0.93	1.68E4	2.79E-4	0.99	1.17E4
2 h	7.24E-6	0.93	1.12E4	3.99E-4	1.00	9.87E3
6 h	9.46E-6	0.92	8.24E3	4.85E-4	1.00	9.96E3
Laser-treated						
0.5 h	1.13E-6	0.76	1.20E5	1.22E-5	0.65	4.13E5
2 h	1.64E-6	0.77	9.24E4	2.74E-5	0.97	1.11E5
6 h	2.17E-6	0.80	6.57E4	4.93E-5	1.00	8.31E4

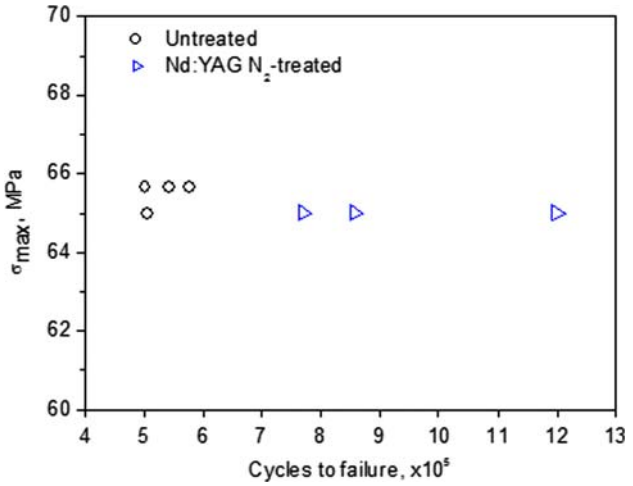

Fig. 11 Corrosion fatigue life of the untreated and laser-treated specimens tested in 3.5% NaCl solution

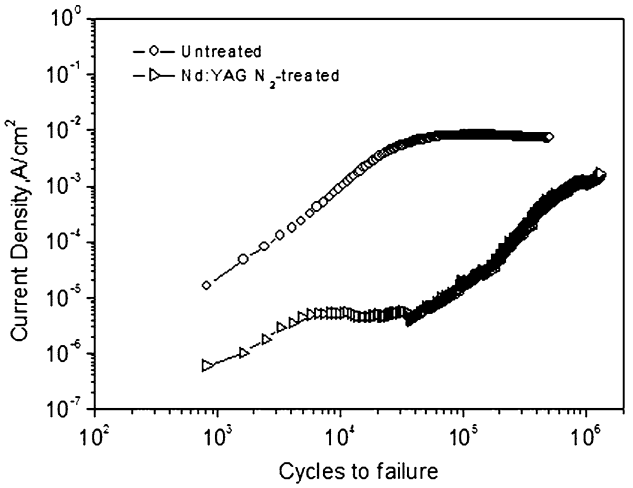

Fig. 12 Current density as a function of fatigue cycle

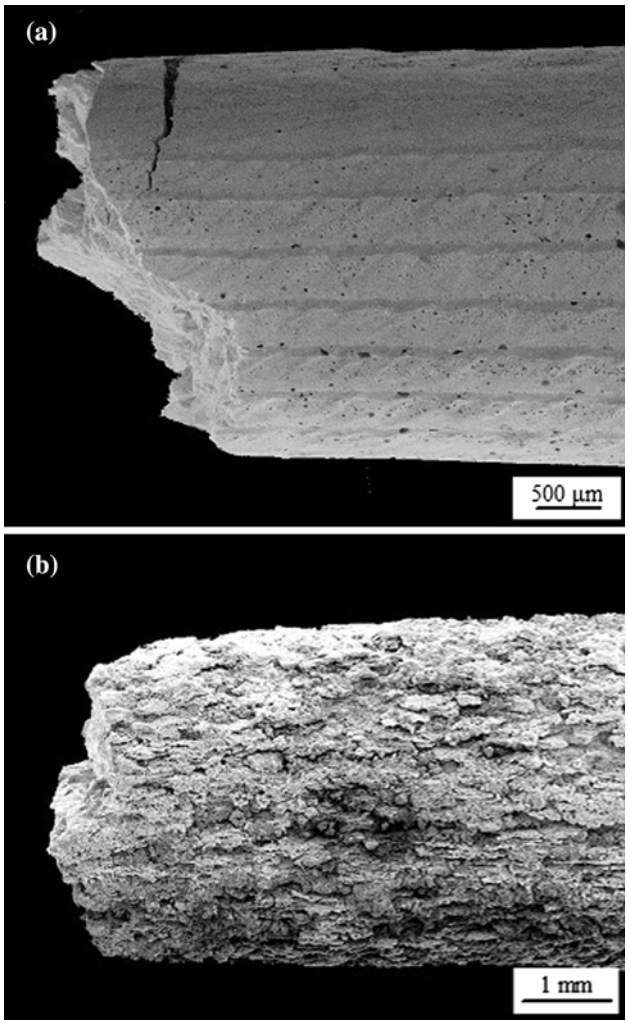

Fig. 13 Condition of the longitudinal surface of (**a**) laser-treated specimen; and (**b**) untreated specimen after the corrosion fatigue test

In this study, the laser tracks are running parallel to the fatigue loading direction, and further studies are required to ascertain the effect of the relationship of laser track orientation and the loading direction on fatigue properties. The effect of the overlapped area of laser tracks and track orientation on corrosion and mechanical properties has been considered previously [24–27]. In general, the overlapped regions were found to be vulnerable to pitting corrosion due to segregation and heterogeneous

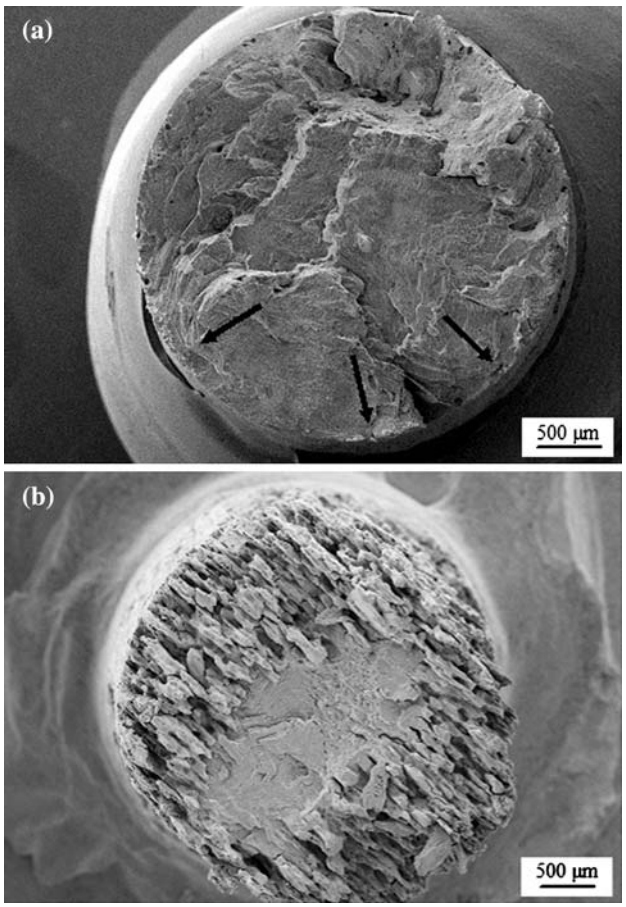

Fig. 14 Fractured surface of (a) laser-treated specimen (the arrows indicate possible fatigue origins), (b) untreated specimen after corrosion fatigue test

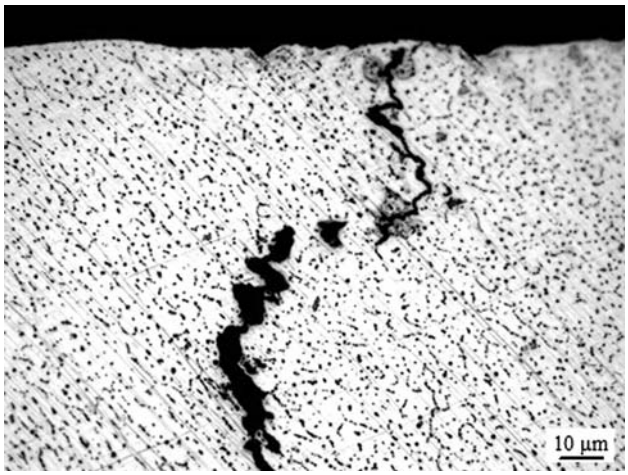

Fig. 15 A cross section of a corrosion fatigue specimen, showing secondary cracks follow an interdendritic path

structures; on the other hand, microcracks could form perpendicular to the track deposition direction. Thus, the effect of track orientation is very much governed by the appearance and the orientation of the defect(s) in relation to the loading direction. Accordingly, it is expected that lower mechanical properties will be obtained if the defects are running perpendicular to the loading direction. In the case of the 6013 alloy when tested under the corrosion fatigue condition, it is considered that, though there may well be such an orientation effect, it may not be as serious as that of some high strength aluminium alloys, such as 2014, in which heavy interdendritic segregation could occur along the track overlapped zone after laser treatment. Moreover, unlike some high strength nickel alloys and steels, cracks and significant phase changes were not detected in the laser tracks and the overlapped areas of the 6013 alloy.

The XRD measurements showed that the residual stress induced by laser treatment was tensile (Table 2). It has been reported that residual tensile stress will facilitate the initiation of fatigue cracking by imposing an extra load on the remote applied load. To confirm the effect of residual stress on fatigue strength, some laser-treated specimens, which had been stress relieved by heat treatment at 180°C were tested. The results showed that the fatigue strength was virtually unchanged. It is considered that the residual stress calculated using the XRD method only measured the stresses in a layer about 5 μm thick [28]. It is highly possible that the tensile stress at the surface is reduced dramatically outside the re-melted layer. Some studies have shown that in laser-treated surfaces, tensile stresses only exist at the very surface of the specimen and the residual stress may even be changed to compressive stress further inside the specimen [29]. Moreover, the TEM observation revealed that LSM formed a layer of nanocrystalline AlN on the surface of the laser-treated specimen. Previous studies reported that thin films of AlN possess an extremely high elastic modulus and strength, of the order of giga-pascals (GPa) [30]. With such a high strength surface coating, it is not surprising that residual tensile stress at the level of 65 MPa would show little effect on crack initiation at the specimen surface. Furthermore, under cyclic loading conditions, residual tensile stresses would relax to a low level with time, and the corresponding detrimental effect on the fatigue behaviour would be alleviated [31]. The results of the present study thus show that the improvement in corrosion resistance brought about by laser surface melting prevailed over the adverse effect caused by the superficial residual stress.

Conclusions

Laser surface melting of aluminium alloy 6013 using a high power Nd:YAG laser was conducted. The two main

objectives of the research have been accomplished. They are: (i) employing laser surface melting to improve the pitting corrosion fatigue resistance of the alloy; and (ii) correlating the characteristics of the microstructure of the laser-modified layers to the behaviour of pitting corrosion fatigue.

Under the conditions of this study, laser surface melting produced a melted layer with a thickness in the range of a few hundred micrometers. Within the layer, fine dendritic structures were formed; coarse second phase particles that were present in the as-received material were eliminated and fine interdendritic phases were formed. When laser melting was conducted in a nitrogen atmosphere, a top surface film, with a thickness of about one micrometer, consisting of the AlN phase was formed.

Turning to corrosion behaviour, electrochemical measurements showed that the pitting corrosion resistance of the 6013 alloy increased after laser surface treatment. This was featured by an increase in corrosion potential and a reduction in corrosion current density. The improvement was attributed to the refinement of the microstructure and the presence of the AlN phase at the surface. With regard to pitting corrosion fatigue, the initiation of fatigue cracks at corrosion pits can be effectively retarded after Nd:YAG laser treatment. Electrochemical measurements recorded during corrosion fatigue testing showed that the current density of the laser-treated specimens was at least one order lower in magnitude than that of the untreated specimens, for the greater part of the fatigue life. Finally, it was found that under the present experimental conditions, the improvement in corrosion resistance brought about by laser surface melting prevailed over the adverse effect caused by the residual stresses induced at the surface of the laser-treated specimens.

Acknowledgements The work described in this article was substantially supported by a grant from the Research Grants Council of the Hong Kong Special Administrative Region, China (Project no. PolyU 5274/03E). The financial support from the Research Committee of the Hong Kong Polytechnic University is also acknowledged.

References

1. Burleigh TD (1991) Corrosion 47:89
2. Stubbington A, Forsyth PJE (1961–1962) J Inst Met 90:347
3. Pao PS, Feng CR, Gill SJ (2000) Corrosion 56:1022
4. Sankaran KK, Perez R, Jata KV (2001) Mater Sci Eng A 297:223
5. Funke AT, Hasson DF, Crowe CR (1981) US naval academy report: corrosion fatigue of anodized aluminum 7075-T73 in salt ladened humid air. Report no.:AD-A103152
6. Watkins KG, McMahon MA, Steen WM (1997) Mater Sci Eng A 231:55
7. McCafferty E, Moore PG, Peace GT (1982) J Electrochem Soc 129:9
8. Chong PH, Liu Z, Skeldon P, Thompson GE (2003) Appl Surf Sci 208–209:399
9. Pao PS, Gill SJ, Feng CR (2000) Scripta Materialia 43:391
10. Burleigh TD (1992) In: Proceedings of the third international conference on aluminium alloys. The Norwegian Institute of Technology, Norway, p 435
11. Blanc C, Mankowski G (1997) Corros Sci 39:949
12. Guillaumin V, Mankowski G (2000) Corrosion 56:12
13. Lin X, Yue TM, Yang HO, Huang WD (2005) Mater Sci Eng A 391:325
14. Guillaumin V, Mankowski G (1999) Corros Sci 41:421
15. Xu WL, Yue TM, Man HC, Chan CP (2006) Surf Coat Technol 200:5077
16. McMahon MA, Green A, Watkins KG, Steen WM, Ferreira MGS, Vilar R (1995) Mater Sci Forum 192–194:789
17. Blanc C, Mankowski G (1997) Corros Sci 39:949
18. Guillaumin V, Mankowski G (2000) Corros Sci 42:105
19. Hsu CH, Mansfeld F (2001) Corrosion 57:747
20. Vasquez MJ, Halada GP, Clayton CR, Longtin JP (2002) Surf Interf Anal 33:607
21. Chan KS, Jones P, Wang QG (2003) Mater Sci Eng A 341:18
22. Suresh S, Ritchie RO (1982) Metallur Transac A 13:1627
23. Kadiri HE, Xue Y, Horstemeyer MF, Jordon JB, Wang PT (2006) Acta Materialia 54:5061
24. Watkins KG, Liu Z, McMahon M, Vilar R, Ferreira MGS (1998) Mater Eng A 252:292
25. Escudero ML, Belló JM (1992) Mater Eng A 158:227
26. Felberbaum L, Voisey K, Gäumann M, Viguier B, Mortensen A (2001) Mater Eng A 299:152
27. Tsay LW, Lin ZW (1998) Fatigue Fract Eng Mater Struct 21:1549
28. Tanner DA, Robinson JS (2006) Mater Sci Technol 22:77
29. Finnie S, Cheng W, Finnie I, Drezet JM, Gremaud M (2003) J Eng Mater Technol 125:302
30. Zong DG, Ong CW, Aravind M, Tsang MP, Choy CL, Lu DR, Ma DJ (2004) Philos Mag 84:3353
31. Juijerm P, Altenberger I, Scholtes B (2006) Mater Eng A 426:4